U.S. DEPARTMENT OF THE INTERIOR
U.S. GEOLOGICAL SURVEY

Comparison of Kinetic-Model Predictions of Deep Gas Generation

by

Allison A. Henry[1]* and Michael D. Lewan[1]

Open File Report No. 99-326

[1]U. S. Geological Survey, Box 25046, MS 977, Denver Federal Center,
Denver, CO 80225 (e-mail: mlewan@usgs.gov)

*Current Address: The Scripps Research Institute, 10550 North Torrey Pines Road, La
Jolla, CA 92037
(e-mail: ahenry@scripps.edu)

INTRODUCTION

The source of and processes resulting in natural gas generation remain a controversial issue in petroleum geochemistry (Price, 1997). Various investigations have used different pyrolysis methods and organic sources to develop models to predict timing and quantities of natural gas generation in sedimentary basins (e.g., Table 1). The results and implications of these different models on predicting natural gas generation have not previously been compared in the literature. The objective of this study is to compare six different published gas-generation kinetic models (Table 1) with respect to their predictions of timing and quantities of deep-gas generation. As discussed by Dyman and others (1997), the potential for deep gas at depths greater than 4,572 meters (15,000ft) remains an uncertain domestic exploration frontier for natural gas. Two geological settings for the occurrence of deep gas emerge from this definition. The first geological setting envisages gas being initially generated and accumulating in traps at shallow depths (< 4,572 m/15,000 ft). As sedimentation and basin subsidence continue with geologic time, these shallow traps remain coherent and are eventually buried to depths greater than 4,572 m (15,000 ft). Deep-gas accumulations resulting from this setting are dependent on the competence of trap closures and seals with burial to depths greater than 4,572 m/15,000 ft. The second geological setting envisages gas generation and accumulation in traps at deeper depths (>4,572 m/15,000 ft). Deep-gas accumulations resulting from this setting are dependent on a source of gas at burial depths greater than 4,572 m/15,000 ft. It is this dependence on sources of deep gas generation that this study examines.

Various kinetic models for the generation of natural gas in sedimentary basins have been published over the last several years. These gas-generation kinetic models are primarily based on different types of laboratory pyrolysis methods, which include open-system anhydrous pyrolysis (e.g., Rock-Eval; Behar and others, 1997), closed-system anhydrous pyrolsis (e.g., microscale sealed (MSSV) pyrolysis; Horsfield and others, 1992), and closed-system hydrous pyrolsis (e.g., flexible gold-bag autoclaves; Knauss and others, 1997). In addition to employing different pyrolysis methods, different starting materials are considered as the source of natural gas. Some kinetic models consider crude oil in deeply buried reservoirs (e.g., Tsuzuki and others, 1997), and others consider unexpelled oil retained in mature source rocks (Pepper and Corvi, 1995).

These kinetic models are examined in two hypothetical basin scenarios that represent end-member heating rates of 1° and 10 °C/m.y. *This study makes no attempt to judge the validity of the six kinetic models used, but only intends to present and compare their results and the implications they have on deep-gas generation.* Kinetic models for the thermal stability of crude oil that are based on model hydrocarbons were not included in this study. Although these studies provide useful information on the influence of pressure, oil matrices, and cracking mechanisms (Domine, 1991; Behar and Vandenbroucke, 1996; Burnham and others, 1997), they are either based on the loss of the model compound rather than generated gas or the generated gases have peculiar gas compositions significantly different from natural gases.

METHODS

Basin Scenarios

Gretener and Curtis (1982) have estimated common heating rates for sedimentary basins to be between 1° and 10 °C/m.y. In keeping with these limits, the kinetic models used in this study are compared in two end-member basin scenarios. One basin scenario uses a thermal gradient of 30°C/km and burial rate of 33.3 m/m.y., which results in a heating rate of 1°C/m.y. The other scenario uses a thermal gradient of 45°C/km and burial rate of 222.2 m/m.y., which results in a heating rate of 10°C/m.y. The heating rates were assumed to be linear in both basin scenarios.

Kinetic Models

Attributes of the six kinetic models considered in this study are given in Table 1. Three of the models consider gas generation from kerogen (Behar and others; 1997, Pepper and Corvi; 1995; and Knauss and others; 1997). Behar and others (1997) used kerogen samples including a type-I kerogen from the Eocene Green River Fm., type-II kerogen from a Toarcian shale of the Paris basin, type-IIS kerogen from the Miocene Monterey Fm., and two type-III kerogens from a Miocene coal in the Mahakam delta and a Dogger coal from the North Sea. Pepper and Corvi (1995) organized their kerogen samples into organofacies A, B, C, D/E, and F. According to their definitions of organofacies, organofacies A kerogen is similar to type-IIS kerogen, organofacies B kerogen is similar to type-II kerogen, organofacies C kerogen is similar to type-I kerogen, organofacies D/E is similar to type III kerogen, and organofacies F is similar to type-III/IV kerogens. Knauss and others (1997) used New Albany Shale (Devonian-Mississippian), which contains type-II kerogen.

The other three models consider gas generation from the cracking of oil (Horsfield and others, 1992; Pepper and Dodd, 1995; and Tsuzuki and others, 1997). Horsfield and others (1992) used of a medium gravity crude oil from a middle Jurassic reservoir in the Central Graben of the Norwegian North Sea (NOCS 33/9-14). Pepper and Dodd (1995) focused on the in-source cracking of oil as opposed to the cracking of reservoir oils; the authors used sixteen samples of source rocks classified as members of their five organofacies. Tsuzuki and others (1997) used a Sarukawa crude oil with an API gravity of 33.6°.

Model/Pyrolysis Terminology

There are four types of models in this study that are based on different pyrolysis methods. The **open pyrolysis** model uses Rock-Eval pyrolysis to determine kinetic parameters (Behar and others, 1997). The **composite pyrolysis** model refers to Pepper and Corvi's (1995) mixed data set from many different references, natural data sets, and open- and closed-system pyrolysis methods. The **anhydrous pyrolysis** model refers to closed-system pyrolysis of kerogen or oil without liquid water and is used by Pepper and Dodd (1995) and Horsfield and others (1992). The **hydrous pyrolysis** model refers to pyrolysis of kerogen or oil in the presence of liquid water and is used by Knauss and others (1997) and Tsuzuki and others (1997).

Extent of Reaction with Single Activation Energy and Frequency Factor

As demonstrated by Wood (1988), the extent of a reaction (i.e., k = rate constant) that follows the Arrhenius equation,

$$k = A \, exp(-E/RT),$$

can be reasonably estimated over a linear heating rate by the approximate analytical integral solution derived by Gorbachev (1975):

$$TTI_{ARR} = \{(A(t_{n+1}-t_n))/(T_{n+1}-T_n)\} * \{[(RT^2_{n+1}/(E+2RT_{n+1}))*exp(-E/RT_{n+1})] - \quad (1)$$
$$[(RT^2_n/(E+2RT_n))*exp(-E/RT_n)]\}$$

where TTI_{ARR} is the extent of reaction function or time-temperature index, A is the frequency factor in m.y.$^{-1}$, E is the activation energy in cal/mol, R is the ideal gas constant in cal/mol-K, t_n is the beginning of the time interval in m.y., t_{n+1} is the end of the time interval in m.y., T_n is the temperature in K at the start of the time interval, and T_{n+1} is the temperature in K at the end of the time interval. TTI_{ARR} can be equated to the integrated first order rate equation,

$$\ln(1/[1-X]) = kt, \quad (2)$$

by

$$TTI_{ARR} = \ln(1/[1-X]) \quad (3)$$

where X represents the extent of reaction as a decimal fraction, which is referred to as fraction of reaction. TTI_{ARR} values can be calculated for various intervals in the burial history of a potential source rock using equation 1. The TTI_{ARR} calculated for each burial interval is additive and the sum values can be converted to fraction of reaction by solving equation 3 for X:

$$X = 1 - (1/exp[TTI_{ARR}]). \quad (4)$$

Tsuzuki and others (1997) derived single E and A values for the generation of C_1-C_5 hydrocarbon gas from the cracking of light (C_6-C_{14} saturates) and heavy (C_{15+} saturates) components of crude oil. The activation energy and frequency factor for the cracking of the light component are respectively 86 kcal/mol and 6.4868 x 10^{35} m.y.$^{-1}$. The activation energy and frequency factor for the cracking of the heavy component are respectively 76 kcal/mol, 3.4187 x 10^{33} m.y.$^{-1}$. These kinetic parameters and the two end-member heating rates were used in equation 1 to determine the extent of gas generation from the cracking of oil in the two basin scenarios.

Extent of Reaction using Multiple Activation Energies or Frequency Factors

In order to reflect a first order reaction with more than one frequency factor or activation energy, X of equation 4 must also represent the fractional extent of reaction for each activation energy and frequency factor. Multiple activation energies or frequency factors are derived by curve-fitting methods that assume first-order parallel reactions. The multiple kinetic parameters are described as discrete or Gaussian distributions, with each of the multiple parameters being assigned a fractional part of the overall reaction (Ungerer and others, 1986; Braum and Burnham, 1987).

The discrete distribution is used by Behar and others (1997) and Horsfield and others (1992). Both groups optimized their experimental kinetic data in such a way to give a variety of activation energies with associated fractions of reaction and a single frequency factor. Behar and others (1997) present discrete activation-energy distributions for the generation of methane (C_1) and C_2-C_5 hydrocarbon gas from five kerogens (Table 2). Horsfield and others (1992) also use a discrete activation-energy distribution between 50 and 73 kcal/mol with a frequency factor of 3.47 x 10^{29} m.y.$^{-1}$ for oil cracking to C_1-C_4 hydrocarbon gas (Table 3). Equation 1 is used for each discrete activation energy for the fractional part of the reaction it is assigned and then summed with results from the other discrete activation energies to give a cumulative generation curve for the extent of reaction.

The Gaussian distribution of activation energies is employed by Pepper and Dodd (1995), Pepper and Corvi (1995), and Knauss and others (1997). The distribution is presented by a mean activation energy, E_{mean}, and a standard deviation, σ_E, as shown in Table 4. A Gaussian distribution is expressed by the equation

$$Y = \frac{1}{\sigma\sqrt{2\pi}} e^{-\frac{1}{2}(X-\mu)^2/\sigma^2}$$ (5)

where σ is the standard deviation at the 68% confidence level (σ_E), μ is the mean activation energy (E_{mean}), and Y is the height of the curve above a given X (discrete activation energy). The function reaches a maximum value of $\frac{1}{\sigma\sqrt{2\pi}}$ when $X = \mu$. Using equation 5 and the parameters given by the cited authors, the Gaussian distribution was divided into discrete 1.0-kcal/mol activation energies. Since the area under the normal curve is one and each rectangle of discrete activation energy is one unit wide, the area of the rectangle becomes the fractional part of the reaction for a given discrete activation energy. When summed, the values at each discrete energy will equal one. Equation 1 is used for each discrete activation energy to determine the fractional part of the reaction it is assigned and then summed with results from the other discrete activation energies to give a cumulative generation curve for the extent of reaction. Pepper and Corvi (1995) and Knauss and others (1997) used a different single frequency factor with each distribution, but Pepper and Dodd (1995) used the same single frequency factor for all of their activation energy distributions (Table 4).

Amount of Gas Generated

All of the kinetic models considered in this study employ first-order reaction rates, which give the extent of reaction, X, as a decimal fraction of the completed reaction at unity (i.e., X equals amount of gas generated at a particular thermal stress divided by the maximum amount of gas that can be generated from a particular source material). The obvious question that remains is how much gas per mass of starting material does unity equal? Behar and others (1997) explicitly state the maximum amounts (i.e., X = 1) of C_1 and C_2-C_5 generated from kerogen as given in Table 5. These values were combined to give maximum yields for C_1-C_5 in milligrams per gram of total organic carbon (mg/g C). Pepper and Corvi (1995) give maximum C_1-C_5 gas generation for each of their five organofacies: A = 105 mg/g C; B = 101 mg/g C; C = 78 mg/g C; D/E = 77 mg/g C; and F = 70 mg/g C.
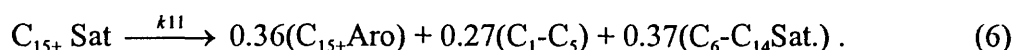
The maximum gas concentrations reported as mmolal for the hydrous pyrolysis experiments by Knauss and others (1997) are converted to mg/g C by the equation

$$\text{Gas (mg/g C)} = \frac{MW \times G_{mmolal} \times \frac{w}{s}}{1000 \times TOC} , \tag{8}$$

where MW is the formula weight of the gas component (i.e., C_1 = 16.04 g/mol, C_2 = 30.07 g/mol, C_3 = 44.10 g/mol, and C_4 = 58.12 g/mol), G_{mmolal} is the maximum gas yield in mmolal (Knauss and others, 1997; Table 2, p.482-483), $\frac{w}{s}$ is the water:shale ratio at time zero for the experiments (i.e., 4.06 g/g), and TOC is the total organic carbon of the rock expressed as a fraction (i.e., 0.114). Equation 8 gives maximum gas yields of 26.5 mg/g C for methane (C_1), 24.9 mg/g C for ethane (C_2), 22.0 mg/g C for propane (C_3) and 19.4 mg/g C for butane (C_4). The total of these values (i.e., 92.8 mg/g C) gives the maximum C_1-C_4 gas generated from the New Albany Shale (Table 5).

According to Pepper and Dodd (1995), the maximum amount of C_1-C_5 gas generated from the cracking of oil in a source rock is equivalent to the amount of oil remaining in the kerogen after expulsion. Therefore, the maximum amount of gas for all sixteen kerogen samples is 100 mg/g C, which they consider the threshold for oil retained by sorption in the kerogen (Pepper, 1998, pers. comm.).

Horsfield and others (1992) experimentally determined that the maximum amount of C_1-C_4 gas generated from the cracking of reservoired oil by closed-system anhydrous pyrolysis is 460 mg/g oil. Tsuzuki and others (1997) considered gas generation from the cracking of reservoired Sarukawa oil by closed-system hydrous pyrolysis. The generation of C_1-C_5 gas is described by two reactions. One reaction (k11) involves the conversion of C_{15+} heavy saturates (C_{15+}Sat) to C_{15+} heavy condensed aromatics (C_{15+}Aro), C_1-C_5 gas (C_1-C_5), and C_6-C_{14} light saturates (C_6-C_{14}Sat):

$$C_{15+}\ \text{Sat} \xrightarrow{k11} 0.36(C_{15+}\text{Aro}) + 0.27(C_1\text{-}C_5) + 0.37(C_6\text{-}C_{14}\text{Sat.}) . \tag{6}$$

The other reaction (k2) involves the conversion of the generated C_6-C_{14} light saturates (C_6-C_{14}Sat) generated in reaction 6 to C_1-C_5 gas (C_1-C_5) and insoluble coke (C_∞):

$$C_6\text{-}C_{14} \text{ sat.} \xrightarrow{k2} 0.60(C_1\text{-}C_5) + 0.40(C_\infty). \qquad (7)$$
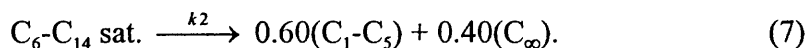
Jamil and others (1991) report that C_{15+} heavy saturates (C_{15+}Sat) comprise 64.9 wt. % of Sarukawa oils. Therefore, one gram of oil will initially generate 175 mg of $C_1\text{-}C_5$ gas through the cracking of C_{15+} heavy saturates (C_{15+}Sat; equation 6) and an additional 144 mg of $C_1\text{-}C_5$ gas through the cracking of $C_6\text{-}C_{14}$ light saturates ($C_6\text{-}C_{14}$Sat; equation 7). These two values are combined to give 319 mg/g oil as the maximum amount of gas generated from the cracking of oil.

RESULTS

Kerogen to Gas

Figure 1 shows the gas-generation curves for Type-I kerogens in basins with 1° and 10 °C/m.y. heating rates as predicted by the open- and composite-pyrolysis models. At the top of the deep gas depth (4,572 m/15,000 ft), 91 and 64% of gas generation from Type-I kerogen is completed at 1°C/m.y. according to the open- and composite-pyrolysis models, respectively. Therefore, 7.9 and 27.9 mg/g C of deep gas is generated according to the open- and composite-pyrolysis models, respectively (Figure 1a and Table 6). Both models predict that the deep gas generation is finished (i.e., X = 0.99) at depths of 6,800 and 5,600 meters (Table 6). At the top of the deep-gas depth (4,572 m/15,000 ft), the open- and composite-pyrolysis models respectively predict 99 and 100% of gas generation from Type-I kerogen is completed at 10°C/m.y. According to these models, essentially no deep gas is generated from Type-I kerogen at this heating rate.

Figure 2 shows the gas-generation curves for Type-II kerogens in basins with 1° and 10 °C/m.y. heating rates as predicted by the open- and composite-pyrolysis models. At the top of the deep-gas depth (4,572 m/15,000 ft), 75, 67, and 35% of gas generation from Type-II kerogen is completed at 1°C/m.y. according to the hydrous-, open-, and composite-pyrolysis models, respectively. These percentages indicate that 23.0, 22.9 and 65.0 mg/g C of deep gas is generated according to the hydrous-, open-, and composite-pyrolysis models, respectively (Figure 2a and Table 6). Deep-gas generation is finished (i.e., X = 0.99) according to these three models at depths of 5,800, 6800, and 7,200 meters (Table 6). At the top of the deep-gas depth (4,572 m/15,000 ft), the open- and composite-pyrolysis models predict 92, 97, 95 and 100% of gas generation from Type-II kerogen is completed at 10°C/m.y., respectively. Therefore, according to these models essentially no significant amounts of deep gas are generated from Type-II kerogen at this heating rate.

Figure 3 shows the gas-generation curves for Type-IIS kerogens in basins with 1° and 10 °C/m.y. heating rates as predicted by the open- and composite-pyrolysis models. At the top of the deep-gas depth (4,572 m/15,000 ft), 74 and 93 % of gas generation from Type-IIS kerogen is completed at 1°C/m.y. according to the open- and composite-pyrolysis models, respectively. Therefore, 17.9 and 7.0 mg/g C of deep gas is generated according to the open- and composite-pyrolysis models, respectively (Figure 3a and Table 6). These models predict that the deep gas generation is finished (i.e., X =

0.99) at depths of 6,400 and 5,000 meters (Table 6). At the top of the deep-gas depth (4,572 m/15,000 ft), the open- and composite-pyrolysis models predict 99 and 100% of gas generation from Type-IIS kerogen is completed at 10°C/m.y., respectively. Therefore, essentially no deep gas is generated from Type-IIS kerogen at this heating rate.

Figure 4 shows the gas-generation curves for Type-III kerogens in basins with 1° and 10 °C/m.y. heating rates as predicted by the open- and composite-pyrolysis models. At the top of the deep-gas depth (4,572 m/15,000 ft), 26 and 3 % of gas generation from Type-III kerogen is completed at 1°C/m.y. according to the open- and composite-pyrolysis models, respectively. Therefore, 39.7 and 73.8 mg/g C of deep gas is generated according to the open- and composite-pyrolysis models, respectively (Figure 4a and Table 6). These models predict that the deep gas generation is finished (i.e., X = 0.99) at depths of 6,400 and 7,000 meters (Table 6). At the top of the deep-gas depth (4,572 m/15,000 ft), the open- and composite-pyrolysis models predict 85 and 92 % of gas generation from Type-III kerogen is completed at 10°C/m.y., respectively. According to these models 7.9 and 6.0 mg/g C of deep gas is generated from Type-II kerogen at this heating rate.

Figure 5 shows the gas-generation curves for more paraffinic Type-III kerogens (Type-III') in basins with 1° and 10 °C/m.y. heating rates as predicted by the open- and composite-pyrolysis models. At the top of the deep-gas depth (4,572 m/15,000 ft), 11 and 3 % of gas generation from Type-III' kerogen is completed at 1°C/m.y. according to the open- and composite-pyrolysis models, respectively. Therefore, 50.6 and 67.7 mg/g C of deep gas is generated according to the open- and composite-pyrolysis models, respectively (Figure 5a and Table 6). These models predict that the deep gas generation is finished (i.e., X = 0.99) at depths of 7,800 and 7,000 meters (Table 6). At the top of the deep-gas depth (4,572 m/15,000 ft), the open- and composite-pyrolysis models predict 74 and 91 % of gas generation from Type-III kerogen is completed at 10°C/m.y., respectively. According to these models 14.9 and 6.0 mg/g C of deep gas is generated from Type-III' kerogen at this heating rate.

Source-Rock Oil to Gas

The anhydrous pyrolysis model by Pepper and Dodd (1995) considers the kinetics of gas generation exclusively from the cracking of unexpelled oil retained in a source rock after the main stages of oil generation and expulsion are completed. Figure 6 shows their model's predicted gas-generation curves for oil retained in 16 source rocks in basins with 1° and 10 °C/m.y. heating rates. These gas-generation curves are similar for all 16 source rocks irrespective of kerogen type or rock mineralogy. As a result, the gas-generation curve of the St Medard (SM) source rock serves as a representative average for this anhydrous pyrolysis model (Table 6). At the top of the deep-gas depth (4,572 m/15,000 ft), 35 % of gas generation from oil retained in a source rock is completed at 1°C/m.y. Therefore 65 mg/g C of deep gas is generated (Figure 5a and Table 6). This model predicts that the deep gas generation is finished (i.e., X = 0.99) at a depth of 6,600 meters (Table 6). At the top of the deep-gas depth (4,572 m/15,000 ft), this models predicts 100 % of gas generation from oil retained in a mature source rock is completed at

10°C/m.y. Therefore, according to this model essentially no deep gas is generated from oil retained in a source rock at this heating rate.

Reservoir Oil to Gas

Generation of gas from the cracking of oil in reservoirs is considered by the anhydrous- and hydrous-pyrolysis models by Horsfield and others (1992) and Tsuzuki and others (1997), respectively. Figure 7 shows the gas-generation curves for reservoir-oil cracking in basins with 1° and 10 °C/m.y. heating rates as predicted by the anhydrous- and hydrous-pyrolysis models. At the top of the deep-gas depth (4,572 m/15,000 ft), 2 and zero % of gas generation from reservoir-oil cracking is completed at 1°C/m.y. according to the anhydrous- and hydrous-pyrolysis models, respectively. Therefore, 449.5 and 320.2 mg/g oil of deep gas is generated according to the closed anhydrous- and hydrous-pyrolysis models, respectively (Figure 7a and Table 6). These models predict that the deep gas generation is finished (i.e., X = 0.99) at depths of 7,600 and 7,400 meters (Table 6). At the top of the deep-gas depth (4,572 m/15,000 ft), the anhydrous- and hydrous-pyrolysis models predict 80 and 53 % of gas generation from reservoir-oil cracking is completed at 10°C/m.y., respectively. According to these models at 10°C/m.y., 459.6 and 320.2 mg/g oil of deep gas is generated from reservoir oil cracking when reservoirs reach depths of 4,200 and 5,200 meters, respectively.

DISCUSSION

Kerogen to Gas

Gas generation from kerogen at deep depths is more likely at slow basin heating rates irrespective of kerogen type or kinetic model (Table 7). At the slow heating rate of 1 °C/m.y., 5 to 75 mg/g C of deep gas can be generated irrespective of kerogen type or kinetic model. In contrast, at the fast heating rate of 10 °C/my, only 0 to 15 mg/g C of deep gas is generated irrespective of kerogen type or kinetic model (Table 7). The implication here is that only a finite amount of gas can be generated from kerogen within a specific thermal-stress interval. Slow heating rates result in lower temperatures at greater depths, which allows this thermal-stress interval to be extended to greater depths within a basin. Therefore, according to these models, deep basins with cooler subsurface temperatures are more likely to generate deep gas from kerogen than deep basins with hotter subsurface temperatures.

For the slow heating rate, the composite-pyrolysis model predicts the greatest amount of deep gas, with values ranging from 5 to 75 mg/g C (Table 7). The open pyrolysis model gives lower values for deep-gas generation with a range from 8 to 51 mg/g C (Table 7). However, at the rapid heating rate, the open-pyrolysis model predicts greater amounts (1 to 15 mg/g C) of deep-gas generation than that predicted by the composite-pyrolysis model (0-7 mg/g C). The hydrous-pyrolysis model for only Type-II kerogen yields no deep gas at the high heating rate and 23 mg/g C of deep gas at the slow heating rate. Obviously, more hydrous-pyrolysis kinetic studies on the other kerogen types are needed.

It would be valuable to compare all the different kerogen types for the three pyrolysis models, but a complete comparison of kerogen types is only possible between

the open- and composite-pyrolysis models. At both heating rates, the open-pyrolysis model predicts an increase in the amount of deep gas generated from Type-I to Type-II to Type-III kerogen. With the exception of Type-IIS kerogen, this trend is also predicted by the composite-pyrolysis model (i.e., Type-I < Type-II < Type-III kerogen). The composite-pyrolysis method predicts that Type-IIS kerogen generates the least amount of deep gas at both heating rates. The implication of this prediction is that deep basins with high-sulfur oils and carbonate source rocks are not good prospects for deep gas. However, in the open-pyrolysis model, type IIS kerogen generates about the same amount of deep gas as Type-II kerogen at both heating rates.

For the slow heating rate, the composite-pyrolysis model predicts more deep gas generation than the open-pyrolysis model for all kerogen types except for Type-IIS kerogen. As an example, three times as much deep-gas generation is predicted by Type-II kerogen in the composite-pyrolysis model than in the open-pyrolysis model. The hydrous-pyrolysis model for deep-gas generation from Type-II kerogen predicts an intermediate value (23 mg/g C) at the low heating rate and the lowest value (0 mg/g C) at the high heating rate relative to the predictions by the composite- and open-pyrolysis models. Type-II kerogen is the most common source of oil and the results presented here (Table 7) suggest that the predicted potential for deep gas from this kerogen type is highly dependent on the pyrolysis model employed.

Type-I kerogen, which is typically associated with lacustrine sequences and source rocks, consistently has low yields of deep-gas generation in both open- and composite-pyrolysis models and at both heating rates (Table 7). These predictions suggest that basins with deeply buried lacustrine source rock sequences are not favorable for deep-gas generation from kerogen. Conversely, Type III kerogen produces more deep gas than the other kerogen types in both the open- and composite-pyrolysis models and for both heating rates. These predictions imply that basins with deeply buried coals are the most favorable for deep-gas generation from kerogen.

Oil to Gas

Deep gas from the cracking of oil retained in a source rock does not depend on kerogen type or lithology according to the anhydrous-pyrolysis model by Pepper and Dodd (1995). Similar to deep-gas generation from kerogen, deep gas from retained oil in source rocks is most favorable at low heating rates (Table 8). At 1°C/m.y., this model predicts amounts of deep-gas generation that are comparable to those predicted by the composite-pyrolysis model for deep-gas generation from Type-II and -III kerogens (Table 8). At the high heating rate, no deep-gas generation from the cracking of retained oil in source rocks is predicted (Table 8). Therefore, at 10°C/m.y., deep-gas generation from kerogen is more favorable than from the retained oil in a source rock.

Anhydrous- and hydrous-pyrolysis models predict that amounts of deep-gas generated from the cracking of reservoir oil are four- to seven-times greater at 1°C/m.y. and six- to twenty-times greater at 10°C/m.y. than the best deep-gas yields obtained from kerogen (Table 7). This difference is readily explained by oil having a higher thermal stability than kerogen. It has also been shown that the thermal stability of oil increases in the presence of liquid water (Hesp and Rigby, 1973), which would be ubiquitous in most

subsurface reservoirs. This increase in stability with water is supported in part by the lower deep-gas yields predicted by the hydrous-pyrolysis model than anhydrous-pyrolysis model at the high heating rate (Table 6). Although the deep-gas yields predicted for the cracking of reservoir oil are considerably higher than those for kerogen, the amount of kerogen in deeply buried source rocks of a sedimentary basin may be several orders of magnitude greater than the amounts of deeply buried reservoir oil.

CONCLUSIONS AND FUTURE STUDIES

1. Basins with slow heating rates, where source rocks subside slowly through low thermal gradients, are more likely to yield deep gas from kerogen than basins with fast heating rates and rapid subsidence of source rock. Because this is one of the most important implications of this study, it would be interesting to compare amounts of deep gas and heating rates from different sedimentary basins. This would involve creating an inventory of heating rates for domestic basins as well as the amount of deep gas recovered to date. A future study of this type can be used to evaluate the validity of the different models used in this study and target basins with high potential for deep gas.

2. According to the open- and composite-pyrolysis models, Type-III kerogen will yield the most deep gas of the three kerogen types irrespective of heating rate. This implies that basins with deeply buried coals are most likely to contain deep gas. A future study comparing deep-gas yields from basins with differing amounts of deeply buried coal would be a useful way of testing this model-based prediction and targeting basins with high potential for deep gas.

3. According to the open- and composite-pyrolysis models, Type-I kerogen has the least or no potential for deep-gas generation. This implies that basins with deeply buried lacustrine source rocks are not likely to contain deep gas. A future study comparing deep-gas yields from basins with differing amounts of deeply-buried lacustrine source rocks would be a useful way of testing this model-based prediction and exclude basins with low potential for deep gas.

4. Cracking of reservoir oil is predicted by the anhydrous- and hydrous-pyrolysis models to generate the most deep gas irrespective of heating rate. Therefore, basins that currently have deeply buried overmature source rocks have the potential of previously having reservoir oil that has since cracked to generate deep gas. The main control for deep-gas accumulations in this geological setting is the original oil trap remaining competent with burial depth. The Gulf Coast offshore and the Anadarko basin may serve as examples of this geological setting. Future studies of these types of basins can further elucidate the factors controlling deep-gas accumulations and target other areas with high potential for deep gas.

5. There are not significant differences between the predicted amount of deep-gas generated from kerogen by the different pyrolysis kinetic models. However, the hydrous-pyrolysis model considers only Type-II kerogen, and more hydrous-pyrolysis

experiments with kinetic models for gas generation from Type-I, Type-IIS, and Type-III kerogens are needed to test this preliminary conclusion.

6. There is a significant difference between the predicted amounts of deep-gas generated from the cracking of reservoir oil by the anhydrous- and hydrous-pyrolysis kinetic models. The kinetic model derived from hydrous pyrolysis indicates that reservoir oil is more thermally stable and that oil cracking to gas requires higher thermal stress levels than those predicted by the anhydrous-pyrolysis model. More experimental work on the cracking of oil in the presence of water is needed. In addition, these future experiments need to consider the effects of commonly occurring reservoir minerals and their surfaces. Experiments published to date on the cracking of reservoir oil have neglected the potential effects of minerals on gas generation.

REFERENCES
Behar, F. and Vandenbroucke, M., 1996, Experimental determination of the rate constants of the n-C_{25} thermal cracking at 120, 400, and 800 bar: Implications for high-pressure/high-temperature prospects: *Energy & Fuels* **10**, 932-940.

Behar, F., Vandenbroucke, M., Tang, Y., Marquis, F. and Espitalie, J., 1997, Thermal cracking of kerogen in open and closed systems: determination of kinetic parameters and stoichiometric coefficients for oil and gas generation: *Org. Geochem.* **26**, p. 321-339.

Braum, R. L. and Burnham, A. K., 1987, Analysis of chemical reactions using a distribution of activation energies and simpler models: *Energy & Fuel* **1**, pp. 153-161.

Burnham, A.K., Gregg, H.R., Ward, R.L., Knauss, K.G., Copenhaver, S.A., Reynolds, J.G., Sanborn, R., 1997, Decomposition kinetics and mechanism of n-hexadecane-1,2-$^{13}C_2$ and dodec-1-ene-1,2-$^{13}C_2$ doped in petroleum and n-hexadecane: *Geochimica et Cosmochimica Acta* **61**, pp. 3725-3737.

Domine, F., 1991, High pressure pyrolysis of n-hexane, 2,4-dimethylpentane and 1-phenylbutane. Is pressure an important geochemical parameter? *Org. Geochem.* **17**, pp. 619-634.

Dyman, T. S., Rice, D. D., and Westcott, P. A., 1997, Introduction in Dyman, T. S., Rice, D. D., and Westcott, P. A., eds., Geological controls of deep natural gas resources in the United States: U. S. Geological Survey Bulletin 2146, p. 3-5.

Gorbachev, V. M., 1975, A solution to the exponential integral in the non-isothermal kinetics for linear heating: Journal of Thermal Analysis 6, p. 349-350.

Gretener, P.E. and Curtis, C.D., 1982, Role of temperature and time on organic metamorphism *Am. Assoc. Petrol. Geol. Bull.* **66**, p. 1124-1129

Hesp , W. and Rigby, D., 1973, The geochemical alteration of hydrocarbons in the presence of water: *Erdol Kohle-Ergas-Petrochem. Brennstoff-Chemie* **26**, p. 70-76.

Horsfield, B., Schenk, H.J., Mills, N. and Welte, D.H., 1992, An investigation of the in-reservoir conversion of oil to gas: compositional and kinetic findings from closed-system programmed-temperature pyrolysis *Advances in Organic Geochemistry*, **19**, p. 191-204

Jamil, A.S.A., Anwar, M.L. and Kiang, E.S.P., 1991, Geochemistry of selected crude oils from Sabah and Sarawak *Geol. Soc. Malaysia Bull.* **28**, p. 123-149

Knauss, K.G., Copenhaver, S.A., Braun, R.L. and Burnham, A.K., 1997, Hydrous pyrolysis of New Albany and Phosphoria Shales: production kinetics of carboxylic acids and light hydrocarbons and interactions between the inorganic and organic chemical systems *Org. Geochem.* **27**, p. 477-496.

Pepper, A.S. and Corvi, P.J., 1995, Simple kinetic models of petroleum formation. Part I: Oil and gas generation from kerogen *Mar. Petrol. Geol.* **12**, p. 291-319

Pepper, A.S. and Dodd, T.A., 1995, Simple kinetic models of petroleum formation. Part II: Oil-gas cracking *Mar. Petrol. Geol.* **12**, p. 321-340

Price, L. C., 1997, Origins, characteristics, evidence for and economic viabilities of conventional and unconventional gas resource bases: *in* Dyman, T. S., Rice, D. D., and Westcott, P. A., eds., Geological controls of deep natural gas resources in the United States: U. S. Geological Survey Bulletin 2146, p. 181-207.

Tsuzuki, N., Yokoyama, Y., Takayama, K., Yokoi, K., Suzuki, M. and Takeda, N. Kinetic modeling of oil cracking, *1997 Eastern Section American Association of Petroleum Geologists* and *The Society of Organic* Petrology Joint Meeting: Lexington, Kentucky; Abstracts and Program, Volume 14, 94-96

Ungerer, P., Espitalié, J, Marquis, F., and Durand, B., 1986, Use of kinetic models of organic matter evolution for the reconstruction of paleotemperatures: in Burruss,

J., ed., *Thermal Modeling in Sedimentary Basins*: Paris, Editions Technip., p. 531-546.

Wood, D. A., 1988, Relationships between thermal maturation indices calculated using Arrhenius equation and Lopatin method: Implications for petroleum exploration: *American Association of Petroleum Geologists Bulletin* **72**, 115-134.

Table 1: Summary of six gas-generation kinetic models considered in this study.

MODEL NAME	REF*	STARTING MATERIAL	KINETIC APPROACH	KINETIC PARAMETERS
Open Pyrolysis	1	Kerogen (Type-I,-II, IIS, III)	Optimization of non-isothermal experiments at different heating rates	Discrete distribution of activation energies with single frequency factor
Composite Pyrolysis	2	Kerogen (Type-I,-II, IIS, III)	Optimization of open and anhydrous pyrolysis and natural data	Gaussian distribution of activation energies with single frequency factor
Hydrous Pyrolysis	3	Kerogen (Type-II)	Optimization of isothermal pyrolysis experiments	Gaussian distribution of activation energies with single frequency factor
	4	Crude Oil (light and heavy saturates)	Optimization of isothermal pyrolysis experiments	Single activation energies and frequency factors for light and heavy saturates
Anhydrous Pyrolysis	5	Crude Oil (36°API gravity)	Optimization of non-isothermal experiments at different heating rates	Discrete distribution of activation energies with single frequency factor
	6	Immature Source Rock (Organofacies A, B, C, D/E, F)	Optimization of isothermal pyrolysis experiments at one temperature	Gaussian distribution of activation energies with single frequency factor

* References: 1 = Behar and others (1997); 2 = Pepper and Corvi (1995); 3 = Knauss and others (1997); 4 = Tsuzuki and others (1997)

5 = Horsfield and others (1992); 6 = Pepper and Dodd (1995)

Table 2: Fractional gas yields assigned to discrete activation energies and single frequency factors used by Behar and others (1997) to model gas generation from kerogen.

FRACTIONAL PART OF TOTAL GAS YIELD

Activation Energy (kcal/mol)	Type-I Kerogen C_1 Fractional Gas Yield	Type-I Kerogen C_2-C_5 Fractional Gas Yield	Type-II Kerogen C_1 Fractional Gas Yield	Type-II Kerogen C_2-C_5 Fractional Gas Yield	Type-IIS Kerogen C_1 Fractional Gas Yield	Type-IIS Kerogen C_2-C_5 Fractional Gas Yield	Type-III' Kerogen C_1 Fractional Gas Yield	Type-III' Kerogen C_2-C_5 Fractional Gas Yield	Type-III Kerogen C_1 Fractional Gas Yield	Type-III Kerogen C_2-C_5 Fractional Gas Yield
74.0	0.00	0.00	0.00	0.00	0.00	0.00	0.00	0.00	0.032	0.00
72.0	0.00	0.00	0.00	0.00	0.00	0.00	0.02	0.00	0.126	0.01
70.0	0.00	0.00	0.00	0.00	0.00	0.00	0.13	0.00	0.133	0.06
68.0	0.00	0.00	0.00	0.002	0.00	0.00	0.16	0.02	0.136	0.05
66.0	0.02	0.00	0.02	0.006	0.004	0.00	0.16	0.04	0.159	0.10
64.0	0.08	0.00	0.07	0.014	0.019	0.00	0.16	0.07	0.155	0.18
62.0	0.08	0.00	0.11	0.024	0.034	0.00	0.14	0.17	0.129	0.25
60.0	0.10	0.00	0.13	0.040	0.174	0.01	0.11	0.28	0.094	0.24
58.0	0.12	0.00	0.19	0.092	0.159	0.03	0.07	0.22	0.032	0.11
56.0	0.19	0.00	0.15	0.225	0.186	0.05	0.03	0.13	0.003	0.02
54.0	0.38	0.95	0.15	0.247	0.144	0.19	0.01	0.05	0.00	0.00
52.0	0.02	0.05	0.11	0.241	0.080	0.27	0.00	0.02	0.00	0.00
50.0	0.00	0.00	0.05	0.092	0.080	0.16	0.00	0.01	0.00	0.00
48.0	0.00	0.00	0.02	0.016	0.068	0.21	0.00	0.00	0.00	0.00
46.0	0.00	0.00	0.00	0.002	0.042	0.06	0.00	0.00	0.00	0.00
44.0	0.00	0.00	0.00	0.00	0.011	0.01	0.00	0.00	0.00	0.00
Frequency Factor (1/m.y.)	2.33E+27	2.33E+27	5.05E+27	5.05E+27	7.88E+26	7.88E+26	9.46E+28	9.46E+28	9.78E+28	9.78E+28
Total gas yields	16.4 mg/g C	72.1 mg/g C	18.8 mg/g C	50.2 mg/g C	26.4 mg/g C	43.9 mg/g C	30.6 mg/g C	23.6 mg/g C	30.9 mg/g C	26.2 mg/g C

16

Table 3: Fractional C_1-C_4 gas yields assigned to discrete activation energies by Horsfield and others (1992) to model gas generation from the cracking of oil.

Activation Energy (kcal/mol)	Fractional Gas Yields
73	0.0174
72	0.0087
70	0.0587
69	0.1109
68	0.1478
67	0.2870
66	0.3435
63	0.0043
58	0.0065
55	0.0022
54	0.0022
53	0.0043
51	0.0022
50	0.0022
Frequency Factor (1/m.y.)	3.47E+29
Total gas yield	460 mg/g Oil

Table 4a: Gaussian distributions and their calculated discrete distributions of activation energies with fractional C_1-C_5 gas yields from kerogens as predicted by the composite pyrolysis model (Pepper and Corvi, 1995).

Organofacies A Type IIS Gaussian Distribution of Activation Energies (kcal/mol)		Organofacies B Type II Gaussian Distribution of Activation Energies (kcal/mol)		Organofacies C Type I Gaussian Distribution of Activation Energies (kcal/mol)		Organofacies F/DE Type III/III' Gaussian Distribution of Activation Energies (kcal/mol)	
mean	49.4	mean	66.6	mean	59.8	mean	65.7
std.dev.	2.6	std.dev.	4.4	std.dev.	2.4	std.dev.	2.4
Discrete Distribution		Discrete Distribution		Discrete Distribution		Discrete Distribution	
Activation Energies (kcal/mol)	Fractional Gas Yield	Activation Energies (kcal/mol)	Fractional Gas Yield	Activation Energies (kcal/mol)	Fractional Gas Yield	Activation Energies (kcal/mol)	Fractional Gas Yield
56.4	0.0037	77.6	0.0040	65.8	0.0079	71.7	0.0070
55.4	0.0100	76.6	0.0069	64.8	0.0201	70.7	0.0185
54.4	0.0231	75.6	0.0112	63.8	0.0432	69.7	0.0412
53.4	0.0460	74.6	0.0174	62.8	0.0782	68.7	0.0766
52.4	0.0785	73.6	0.0257	61.8	0.1191	67.7	0.1191
51.4	0.1150	72.6	0.0359	60.8	0.1529	66.7	0.1549
50.4	0.1446	71.6	0.0477	59.8	0.1652	65.7	0.1686
49.4	0.1560	70.6	0.0601	58.8	0.1504	64.7	0.1535
48.4	0.1445	69.6	0.0720	57.8	0.1154	63.7	0.1168
47.4	0.1148	68.6	0.0819	56.8	0.0745	62.7	0.0744
46.4	0.0783	67.6	0.0885	55.8	0.0405	61.7	0.0396
45.4	0.0458	66.6	0.0907	54.8	0.0186	60.7	0.0177
44.4	0.0230	65.6	0.0884	53.8	0.0072	59.7	0.0066
43.4	0.0099	64.6	0.0817	52.8	0.0000	58.7	0.0000
42.4	0.0037	63.6	0.0718	51.8	0.0000	57.7	0.0000
41.5	0.0000	62.6	0.0598	50.8	0.0000	56.7	0.0000
40.5	0.0000	61.6	0.0474	49.8	0.0000	55.7	0.0000
39.5	0.0000	60.6	0.0356	48.8	0.0000	54.7	0.0000
38.5	0.0000	59.6	0.0255	47.8	0.0000	53.7	0.0000
37.5	0.0000	58.6	0.0173	46.8	0.0000	52.7	0.0000
36.5	0.0000	57.6	0.0111	45.8	0.0000	51.7	0.0000
35.5	0.0000	56.6	0.0068	44.8	0.0000	50.7	0.0000
34.5	0.0000	55.6	0.0039	43.8	0.0000	49.7	0.0000
Frequency Factor (1/m.y.)	1.24E+26		6.84E+31		7.22E+29		6.09E+29

Table 4b: Gaussian distributions and their calculated discrete distributions of activation energies with fractional C1-C5 gas yield from oil retained in mature source rocks as predicted by the anhydrous pyrolysis model (Pepper and Dodd, 1995). The frequency factor (1/m.y.) for all source rocks is 3.15×10^{27}. Source rock abbreviations are given in caption of Figure 6.

Source Rock

Gaussian Distribution	BL	SM
Activation Energies (kcal/mol)		
mean	58.7	57.7
std. dev.	1.7	2.9

Discrete Distribution	Fractional Gas Yield	
Activation Energy (kcal/mol)	BL	SM
65.7	0.0000	0.0030
64.7	0.0000	0.0073
63.7	0.0026	0.0161
62.7	0.0132	0.0313
61.7	0.0466	0.0537
60.7	0.1147	0.0818
59.7	0.1977	0.1102
58.7	0.2384	0.1316
57.7	0.2011	0.1391
56.7	0.1187	0.1302
55.7	0.0490	0.1079
54.7	0.0142	0.0792
53.7	0.0029	0.0515
52.7	0.0000	0.0296
51.7	0.0000	0.0151
50.7	0.0000	0.0068
49.7	0.0000	0.0027
48.7	0.0000	0.0000
47.7	0.0000	0.0000
46.7	0.0000	0.0000
45.7	0.0000	0.0000
44.7	0.0000	0.0000

Source Rock

Gaussian Distribution	AWD	Ha
Activation Energies (kcal/mol)		
mean	58.4	56.4
std. dev.	2.4	3.6

Discrete Distribution	Fractional Gas Yield	
Activation Energy (kcal/mol)	AWD	Ha
68.4	0.0000	0.0000
67.4	0.0000	0.0000
66.4	0.0000	0.0000
65.4	0.0022	0.0048
64.4	0.0069	0.0093
63.4	0.0182	0.0166
62.4	0.0401	0.0275
61.4	0.0745	0.0422
60.4	0.1162	0.0598
59.4	0.1520	0.0785
58.4	0.1669	0.0953
57.4	0.1538	0.1071
56.4	0.1190	0.1113
55.4	0.0773	0.1070
54.4	0.0422	0.0952
53.4	0.0193	0.0783
52.4	0.0074	0.0596
51.4	0.0024	0.0420
50.4	0.0000	0.0274
49.4	0.0000	0.0155
48.4	0.0000	0.0092
47.4	0.0000	0.0047

Source Rock

Gaussian Distribution	PAL	LC9	Ta	CO
Activation Energies (kcal/mol)				
mean	58.1	57.1	58.1	57.1
std. dev.	2.2	3.6	2.6	2.4

Discrete Distribution	Fractional Gas Yield			
Activation Energy (kcal/mol)	PAL	LC9	Ta	CO
68.1	0.0000	0.0000	0.0000	0.0000
67.1	0.0000	0.0022	0.0000	0.0000
66.1	0.0000	0.0046	0.0000	0.0000
65.1	0.0000	0.0089	0.0043	0.0000
64.1	0.0037	0.0161	0.0110	0.0024
63.1	0.0122	0.0268	0.0245	0.0073
62.1	0.0323	0.0413	0.0471	0.0191
61.1	0.0691	0.0588	0.0784	0.0418
60.1	0.1193	0.0775	0.1129	0.0768
59.1	0.1657	0.0945	0.1407	0.1185
58.1	0.1855	0.1066	0.1517	0.1535
57.1	0.1672	0.1113	0.1416	0.1669
56.1	0.1215	0.1074	0.1143	0.1523
55.1	0.0711	0.0960	0.0799	0.1167
54.1	0.0335	0.0793	0.0483	0.0750
53.1	0.0127	0.0606	0.0253	0.0405
52.1	0.0039	0.0429	0.0114	0.0184
51.1	0.0000	0.0281	0.0045	0.0070
50.1	0.0000	0.0170	0.0000	0.0022
49.1	0.0000	0.0095	0.0000	0.0000
48.1	0.0000	0.0049	0.0000	0.0000
47.1	0.0000	0.0024	0.0000	0.0000

Table 4b: *(Continued)*

Source Rock	LC1	Tu
Gaussian Distribution		
Activation Energies (kcal/mol)		
mean	57.3	58.3
std. dev.	2.9	2.4

Discrete Distribution

Activation Energy (kcal/mol)	Fractional Gas Yield	
68.3	0.0000	0.0000
67.3	0.0000	0.0000
66.3	0.0000	0.0000
65.3	0.0028	0.0023
64.3	0.0069	0.0073
63.3	0.0152	0.0190
62.3	0.0298	0.0416
61.3	0.0517	0.0766
60.3	0.0795	0.1183
59.3	0.1082	0.1534
58.3	0.1303	0.1669
57.3	0.1391	0.1525
56.3	0.1314	0.1169
55.3	0.1100	0.0752
54.3	0.0815	0.0406
53.3	0.0535	0.0184
52.3	0.0311	0.0070
51.3	0.0160	0.0022
50.3	0.0073	0.0000
49.3	0.0029	0.0000
48.3	0.0000	0.0000
47.3	0.0000	0.0000
46.3	0.0000	0.0000

Source Rock	GA	KFC	P5	Maui	WE
Gaussian Distribution					
Activation Energies (kcal/mol)					
mean	56.6	58.6	58.6	57.6	57.6
std. dev.	4.8	2.6	1.9	3.6	4.3

Discrete Distribution

Activation Energy (kcal/mol)	Fractional Gas Yield				
68.6	0.0037	0.0000	0.0000	0.0000	0.0035
67.6	0.0060	0.0000	0.0000	0.0023	0.0062
66.6	0.0095	0.0000	0.0000	0.0048	0.0104
65.6	0.0144	0.0042	0.0000	0.0092	0.0165
64.6	0.0209	0.0108	0.0014	0.0165	0.0247
63.6	0.0290	0.0241	0.0064	0.0274	0.0351
62.6	0.0384	0.0465	0.0223	0.0421	0.0472
61.6	0.0488	0.0776	0.0588	0.059	0.0602
60.6	0.0593	0.1122	0.1179	0.0784	0.0727
59.6	0.0689	0.1402	0.1798	0.0952	0.0832
58.6	0.0768	0.1517	0.2086	0.107	0.0903
57.6	0.0818	0.1420	0.1841	0.1113	0.0927
56.6	0.0835	0.1150	0.1236	0.1070	0.0903
55.6	0.0815	0.0806	0.0631	0.0952	0.0832
54.6	0.0762	0.0489	0.0245	0.0784	0.0727
53.6	0.0681	0.0257	0.0072	0.0597	0.0602
52.6	0.0583	0.0117	0.0016	0.0421	0.0472
51.6	0.0478	0.0046	0.0000	0.0274	0.0351
50.6	0.0375	0.0000	0.0000	0.0165	0.0247
49.6	0.0282	0.0000	0.0000	0.0092	0.0165
48.6	0.0203	0.0000	0.0000	0.0048	0.0104
47.6	0.0139	0.0000	0.0000	0.0023	0.0062
46.6	0.0092	0.0000	0.0000	0.0000	0.0035

Source Rock	P4
Gaussian Distribution	
Activation Energies (kcal/mol)	
mean	58.8
std. dev.	1.2

Discrete Distribution

Activation Energy (kcal/mol)	Fractional Gas Yield
68.8	0.0000
67.8	0.0000
66.8	0.0000
65.8	0.0000
64.8	0.0000
63.8	0.0000
62.8	0.0012
61.8	0.0142
60.8	0.0818
59.8	0.2345
58.8	0.3338
57.8	0.2360
56.8	0.0828
55.8	0.0144
54.8	0.0012
53.8	0.0000
52.8	0.0000
51.8	0.0000
50.8	0.0000
49.8	0.0000
48.8	0.0000
47.8	0.0000
46.8	0.0000

Table 4c: Gaussian distributions and their calculated discrete distributions of activation energies with fractional methane (C_1), ethane (C_2), propane (C_3), and butane (C_4) yields from Type-II kerogen in the New Albany Shale (Devonian-Mississippian) as predicted by the hydrous-pyrolysis model (Knauss and others, 1997).

Methane (C_1)		Ethane (C_2)		Propane (C_3)		Butane (C_4)	
Gaussian Distribution		Gaussian Distribution		Gaussian Distribution		Gaussian Distribution	
E (kcal/mol) 45.2		E (kcal/mol) 56.2		E (kcal/mol) 52.9		E (kcal/mol) 55.0	
std. dev.(%E) 1.92		std. dev.(%E) 5.0		std. dev.(%E) 6.0		std. dev.(%E) 5.0	
Discrete Distributon		Discrete Distributon		Discrete Distributon		Discrete Distributon	
Activation Energies (kcal/mol)	Fractional Gas Yield	Activation Energies (kcal/mol)	Fractional Gas Yield	Activation Energies (kcal/mol)	Fractional Gas Yield	Activation Energies (kcal/mol)	Fractional Gas Yield
65.4	0.0000	65.2	0.0008	64.9	0.0000	65.0	0.0000
64.4	0.0000	64.2	0.0025	63.9	0.0000	64.0	0.0007
63.4	0.0000	63.2	0.0064	62.9	0.0009	63.0	0.0021
62.4	0.0000	62.2	0.0145	61.9	0.0023	62.0	0.0057
61.4	0.0000	61.2	0.0292	60.9	0.0052	61.0	0.0134
60.4	0.0000	60.2	0.0515	59.9	0.0110	60.0	0.0278
59.4	0.0000	59.2	0.0803	58.9	0.0211	59.0	0.0504
58.4	0.0000	58.2	0.1102	57.9	0.0363	58.0	0.0800
57.4	0.0000	57.2	0.1333	56.9	0.0568	57.0	0.1114
56.4	0.0000	56.2	0.1420	55.9	0.0804	56.0	0.1358
55.4	0.0000	55.2	0.1333	54.9	0.1031	55.0	0.1451
54.4	0.0000	54.2	0.1102	53.9	0.1196	54.0	0.1358
53.4	0.0000	53.2	0.0803	52.9	0.1257	53.0	0.1114
52.4	0.0000	52.2	0.0515	51.9	0.1196	52.0	0.0800
51.4	0.0000	51.2	0.0292	50.9	0.1031	51.0	0.0504
50.4	0.0000	50.2	0.0145	49.9	0.0804	50.0	0.0278
49.4	0.0000	49.2	0.0064	48.9	0.0568	49.0	0.0134
48.4	0.0012	48.2	0.0025	47.9	0.0363	48.0	0.0057
47.4	0.0329	47.2	0.0008	46.9	0.0211	47.0	0.0021
46.4	0.2370	46.2	0.0000	45.9	0.0110	46.0	0.0007
45.4	0.4577	45.2	0.0000	44.9	0.0052	45.0	0.0000
44.4	0.2370	44.2	0.0000	43.9	0.0023	44.0	0.0000
43.4	0.0329	43.2	0.0000	42.9	0.0009	43.0	0.0000
42.4	0.0012	42.2	0.0000	41.9	0.0000	42.0	0.0000
Frequency Factor (1/m.y.) 7.88E+23		1.23E+28		5.68E+26		3.15E+27	

Table 5: Maximum C_1-C_5 gas yields for different starting materials used in six kinetic models.

Starting Material	Model Reference*	Maximum Gas Yield (mg/g C)
Type-I Kerogen	1	88.5
	2	78.0
Type-II Kerogen	1	70.0
	2	100.6
	3	92.8**
Type-IIS Kerogen	1	70.3
	2	104.9
Type-III Kerogen	1	57.1
	2	76.6
Type-III' Kerogen	1	54.2
	2	69.5
Source-Rock Oil	4	100.00
Reservoir Oil	5	541.2
	(mg/g Oil)	*(460.0)*
	6	376.2
	(mg/g Oil)	*(319.8)*

* References: 1 = Behar and others (1997)
                 2 = Pepper and Corvi (1995)
                 3 = Knauss and others (1997)
                 4 = Pepper and Dodd (1995)
                 5 = Horsfield and others (1992)
                 6 = Tsuzuki and others (1997)

**C_1-C_4

Table 6: Summary of gas generation-curves for kerogens and oils (Figures 1-6) with respect to yield, depth, time, and temperature for fraction of reaction values of 0.05, 0.25, 0.50, 0.75, and 0.99 at 1 and 10°C/m.y. heating rates for each kinetic model. Last column of each heating rate gives the fraction of reaction, yield, time, and temperature at the start of deep gas (15,000ft/4,572 m).

Type-I Kerogen

Open-Pyrolysis Model[1]

	1°C/m.y.						10°C/m.y.					
Fraction of Reaction (X)	0.050	0.250	0.500	0.750	0.990	0.909	0.050	0.250	0.500	0.750	0.990	0.989
Gas Yield (mg/g C)	4	22	44	66	87	80	4	22	44	66	87	87
(ft³/kg C)	0.168	0.840	1.680	2.520	3.326	3.054	0.168	0.840	1.680	2.520	3.326	3.321
Depth (m)	3600	4000	4200	4200	6800	4572	2400	2600	2800	3000	4572	4572
Time (m.y.)	108	120	126	126	204	137	11	12	13	14	21	21
Temperature (°C)	128	140	146	146	224	157	128	137	146	155	226	226

Composite-Pyrolysis Model[2]

	1°C/m.y.						10°C/m.y.					
Fraction of Reaction (X)	0.050	0.250	0.500	0.750	0.990	0.641	0.050	0.250	0.500	0.750	0.990	1.000
Gas Yield (mg/g C)	4	20	39	59	77	78	4	20	39	59	77	78
(ft³/kg C)	0.149	0.744	1.489	2.233	2.948	2.978	0.149	0.744	1.489	2.233	2.948	2.978
Depth (m)	3400	4000	4400	4800	5600	4572	2400	2600	3000	3400	4000	4572
Time (m.y.)	102	120	132	144	168	137	11	12	14	15	18	21
Temperature (°C)	122	140	152	164	188	157	128	137	155	173	200	226

Type-II Kerogen

Open-Pyrolysis Model[1]

	1°C/m.y.						10°C/m.y.					
Fraction of Reaction (X)	0.050	0.250	0.500	0.750	0.990	0.671	0.050	0.250	0.500	0.750	0.990	0.971
Gas Yield (mg/g C)	4	18	35	53	69	47	4	18	35	53	69	68
(ft³/kg C)	0.134	0.668	1.336	2.004	2.645	1.794	0.134	0.668	1.336	2.004	2.645	2.596
Depth (m)	2800	3600	4200	4800	6800	4572	1800	2400	2800	3200	4800	4572
Time (m.y.)	84	108	126	144	204	137	8	11	13	14	22	21
Temperature (°C)	104	128	146	164	224	157	101	128	146	164	236	226

Composite-Pyrolysis Model[2]

	1°C/m.y.						10°C/m.y.					
Fraction of Reaction (X)	0.050	0.250	0.500	0.750	0.990	0.350	0.050	0.250	0.500	0.750	0.990	0.950
Gas Yield (mg/g C)	5	25	50	75	99	35	5	25	50	75	99	95
(ft³/kg C)	0.191	0.954	1.909	2.863	3.779	1.336	0.191	0.954	1.909	2.863	3.779	3.627
Depth (m)	3400	4400	5000	5600	7200	4572	2400	3000	3400	3800	5000	4572
Time (m.y.)	102	132	150	168	216	137	11	14	15	17	23	21
Temperature (°C)	122	152	170	188	236	157	128	155	173	191	245	226

Hydrous-Pyrolysis Model[3]

	1°C/m.y.						10°C/m.y.					
Fraction of Reaction (X)	0.050	0.250	0.500	0.750	0.990	0.753	0.050	0.250	0.500	0.750	0.990	1.000
Gas Yield (mg/g C)	5	23	47	70	92	70	5	23	47	70	92	93
(ft³/kg C)	0.180	0.899	1.797	2.696	3.559	2.706	0.180	0.899	1.797	2.696	3.559	3.595
Depth (m)	2800	3400	3800	4572	5800	4572	2000	2400	2800	3200	4000	4572
Time (m.y.)	84	102	114	137	174	137	9	11	13	14	18	21
Temperature (°C)	104	122	134	157	194	157	110	128	146	164	200	226

23

Table 6 (*continued*)

Type-IIS Kerogen

Open-Pyrolysis Model[1]

	1°C/m.y.						10°C/m.y.					
Fraction of Reaction (X)	0.050	0.250	0.500	0.750	0.990	0.743	0.050	0.250	0.500	0.750	0.990	0.986
Gas Yield (mg/g C)	4	18	35	53	69	52	4	18	35	53	69	69
(ft³/kg C)	0.134	0.668	1.336	2.004	2.645	1.985	0.134	0.668	1.336	2.004	2.645	2.634
Depth (m)	2400	3000	4000	4572	6400	4572	1600	2200	2800	3200	4572	4572
Time (m.y.)	72	90	120	137	192	137	7	10	13	14	21	21
Temperature (°C)	92	110	140	157	212	157	92	119	146	164	226	226

Composite-Pyrolysis Model[2]

	1°C/m.y.						10°C/m.y.					
Fraction of Reaction (X)	0.050	0.250	0.500	0.750	0.990	0.933	0.050	0.250	0.500	0.750	0.990	1.000
Gas Yield (mg/g C)	5	26	53	79	104	98	5	26	53	79	104	105
(ft³/kg C)	0.200	1.002	2.004	3.006	3.968	3.741	0.200	1.002	2.004	3.006	3.968	4.008
Depth (m)	2400	3000	3400	4000	5000	4572	1600	2000	2400	2800	3600	4572
Time (m.y.)	72	90	102	120	150	137	7	9	11	13	16	21
Temperature (°C)	92	110	122	140	170	157	92	110	128	146	182	226

Type-III Kerogen

Open-Pyrolysis Model[1]

	1°C/m.y.						10°C/m.y.					
Fraction of Reaction (X)	0.050	0.250	0.500	0.750	0.990	0.259	0.050	0.250	0.500	0.750	0.990	0.852
Gas Yield (mg/g C)	3	14	27	41	53	14	3	14	27	41	53	46
(ft³/kg C)	0.000103	0.000515	0.001031	0.001546	0.002041	0.000534	0.000103	0.000515	0.001031	0.001546	0.002041	0.001756
Depth (m)	3600	4400	5200	6200	7400	4572	2400	3200	3600	4200	5200	4572
Time (m.y.)	108	132	156	186	222	137	11	14	16	19	23	21
Temperature (°C)	128	152	176	206	242	157	128	164	182	209	254	226

Composite-Pyrolysis Model[2]

	1°C/m.y.						10°C/m.y.					
Fraction of Reaction (X)	0.050	0.250	0.500	0.750	0.990	0.026	0.050	0.250	0.500	0.750	0.990	0.921
Gas Yield (mg/g C)	4	19	38	57	75	2	4	19	38	57	75	70
(ft³/kg C)	0.145	0.725	1.451	2.176	2.872	0.076	0.145	0.725	1.451	2.176	2.872	2.672
Depth (m)	4800	5400	5800	6000	7000	4572	3200	3600	4000	4200	4800	4800
Time (m.y.)	144	162	174	180	210	137	14	16	18	19	22	21
Temperature (°C)	164	182	194	200	230	157	164	182	200	209	236	226

Type-III' Kerogen

Open-Pyrolysis Model[1]

	1°C/m.y.						10°C/m.y.					
Fraction of Reaction (X)	0.050	0.250	0.500	0.750	0.990	0.105	0.050	0.250	0.500	0.750	0.990	0.737
Gas Yield (mg/g C)	3	14	29	43	56	6	3	14	29	43	56	42
(ft³/kg C)	0.109	0.544	1.088	1.632	2.154	0.229	0.109	0.544	1.088	1.632	2.154	1.603
Depth (m)	4200	5000	5800	6600	7800	4572	3000	3400	4000	4572	5600	4572
Time (m.y.)	126	150	174	198	234	137	14	15	18	21	25	21
Temperature (°C)	146	170	194	218	254	157	155	173	200	226	272	226

Table 6 (*continued*)

Type-III' Kerogen

Composite-Pyrolysis Model[2]

Parameter		1°C/m.y.						10°C/m.y.				
Fraction of Reaction (X)	0.050	0.250	0.500	0.750	0.990	0.029	0.050	0.250	0.500	0.750	0.990	0.914
Gas Yield (mg/g C)	4	18	35	53	69	2	4	18	35	53	69	64
(ft/kg C)	0.134	0.668	1.336	2.004	2.645	0.076	0.134	0.668	1.336	2.004	2.645	2.443
Depth (m)	4600	5400	5800	6000	7000	4572	3200	3600	4000	4200	4800	4572
Time (m.y.)	138	162	174	180	210	137	14	16	18	19	22	21
Temperature (°C)	158	182	194	200	230	157	164	182	200	209	236	226

Oil in Source Rock

Anhydrous-Pyrolysis Model[4]

Parameter		1°C/m.y.						10°C/m.y.				
Fraction of Reaction (X)	0.050	0.250	0.500	0.750	0.990	0.353	0.050	0.250	0.500	0.750	0.990	1.000
Gas Yield (mg/g C)	5	25	50	75	99	35	5	25	50	75	99	100
(ft/kg C)	0.191	0.954	1.909	2.863	3.779	1.347	0.191	0.954	1.909	2.863	3.779	3.817
Depth (m)	3600	4400	5000	5400	6600	4572	2400	3000	3400	3800	4200	4572
Time (m.y.)	108	132	150	162	198	137	11	14	15	17	19	21
Temperature (°C)	128	152	170	182	218	157	128	155	173	191	209	226

Oil in Reservoirs

Anhydrous-Pyrolysis Model[5]

Parameter		1°C/m.y.						10°C/m.y.				
Fraction of Reaction (X)	0.050	0.250	0.500	0.750	0.990 at 15,000 ft	0.022	0.050	0.250	0.500	0.750	0.990 at 15,000 ft	0.804
Gas Yield (mg/g Oil)	23	115	230	345	455		23	115	230	345	455	
(ft/kg Oil)	0.889	4.445	8.890	13.336	17.603	0.001	0.889	4.445	8.890	13.336	17.603	0.031
Depth (m)	5400	6000	6200	6400	7600	4572	3800	4000	4200	4400	5000	4572
Time (m.y.)	162	180	186	192	228	137	17	18	19	20	23	21
Temperature (°C)	182	200	206	212	248	157	191	200	209	218	245	226

Anhydrous-Pyrolysis Model[6]

Parameter		1°C/m.y.						10°C/m.y.				
Fraction of Reaction (X)	0.050	0.250	0.500	0.750	0.990	0.000	0.050	0.250	0.500	0.750	0.990	0.531
Gas Yield (mg/g Oil)	16	80	160	240	317	0.000	16	80	160	240	317	170.000
(ft/kg Oil)	0.000611	0.003054	0.006108	0.009162	0.012094	0.000	0.000611	0.003054	0.006108	0.009162	0.012094	0.006490
Depth (m)	5800	6200	6400	7200	7400	4572	4000	4200	4400	5000	5200	4572
Time (m.y.)	174	186	192	216	222	137	18	19	20	23	23	21
Temperature (°C)	194	206	212	236	242	157	200	209	218	245	254	226

[1]Behar and others (1997); [2]Pepper and Corvi (1995); [3]Knauss and others (1997); [4]Pepper and Dodd (1995); [5]Horsfield and others (1992); [6]Tsuzuki and others (1997)

Table 7: Amounts of gas generated from kerogen above and below the deep-gas depth of 4,572 m (15,000 ft). All values refer to C_1-C_5 gas, except where otherwise noted.

Kinetic Model	Kerogen Type	1 °C/my Gas Generated		10 °C/my Gas Generated	
		Above 4572 m (mg/g C)	Below 4572 m (mg/g C)	Above 4572 m (mg/g C)	Below 4572 m (mg/g C)
Open Pyrolysis[1]	Type I	80	8	87	1
	Type II	50	20	68	2
	Type IIS	50	20	69	1
	Type III	6	51	42	15
	Type III'	14	40	46	8
Composite Pyrolysis[2]	Type I	50	28	78	0
	Type II	35	65	95	5
	Type IIS	100	5	105	0
	Type III	2	75	70	7
	Type III'	2	68	64	6
Hydrous Pyrolysis[3]	Type II	70*	23*	93*	0*

* All total gas is defined as C_1-C_5 except in these cases, where it is defined as C_1-C_4.

[1] Behar and others (1997); [2] Pepper and Corvi (1995); [3] Knauss and others (1997)

26

Table 8: Amounts of gas generated from kerogen above and below the deep-gas depth of 4,572 m (15,000 ft). All values refer to C_1-C_5 gas, except where otherwise noted.

Kinetic Model	Oil Type	1 °C/my — Gas Generated		10 °C/my — Gas Generated	
		Above 4572 m	Below 4572 m	Above 4572 m	Below 4572 m
Source-Rock Oil		(mg/g C)	(mg/g C)	(mg/g C)	(mg/g C)
Anhydrous Pyrolysis[4]	Oil in Source Rock*	29	71	100	0
		Above 4572 m	Below 4572 m	Above 4572 m	Below 4572 m
Reservoir Oil		(mg/g Oil)	(mg/g Oil)	(mg/g Oil)	(mg/g Oil)
Anhydrous Pyrolysis[5]	North Sea (36° API)	2*	458*	370*	90*
Hydrous Pyrolysis[6]	Sarukawa (33.6° API)	0	320	170	150

* All total gas is defined as C1-C5 except in these cases, where it is defined as C1-C4.

[4] Pepper and Dodd (1995); [5] Horsfield et al. (1992); [6] Tsuzuki et al. (1997)
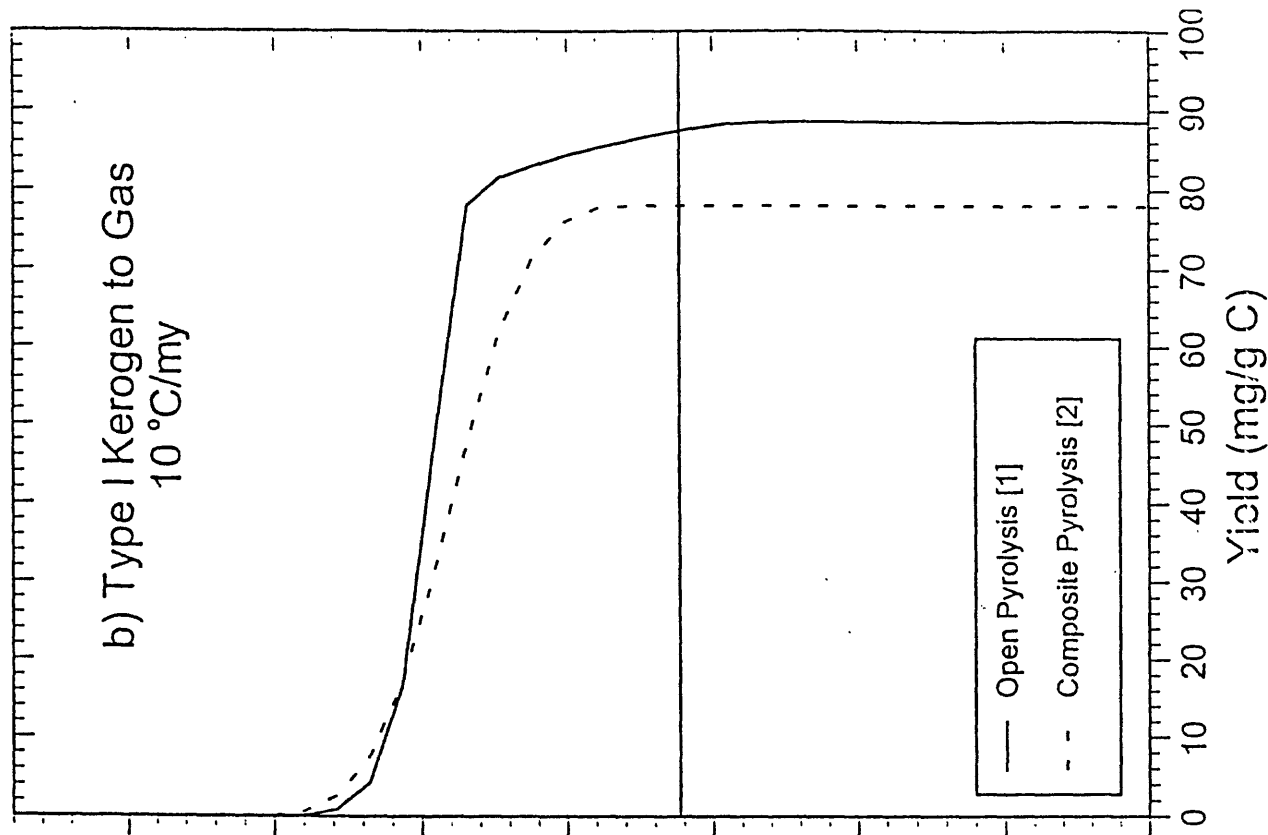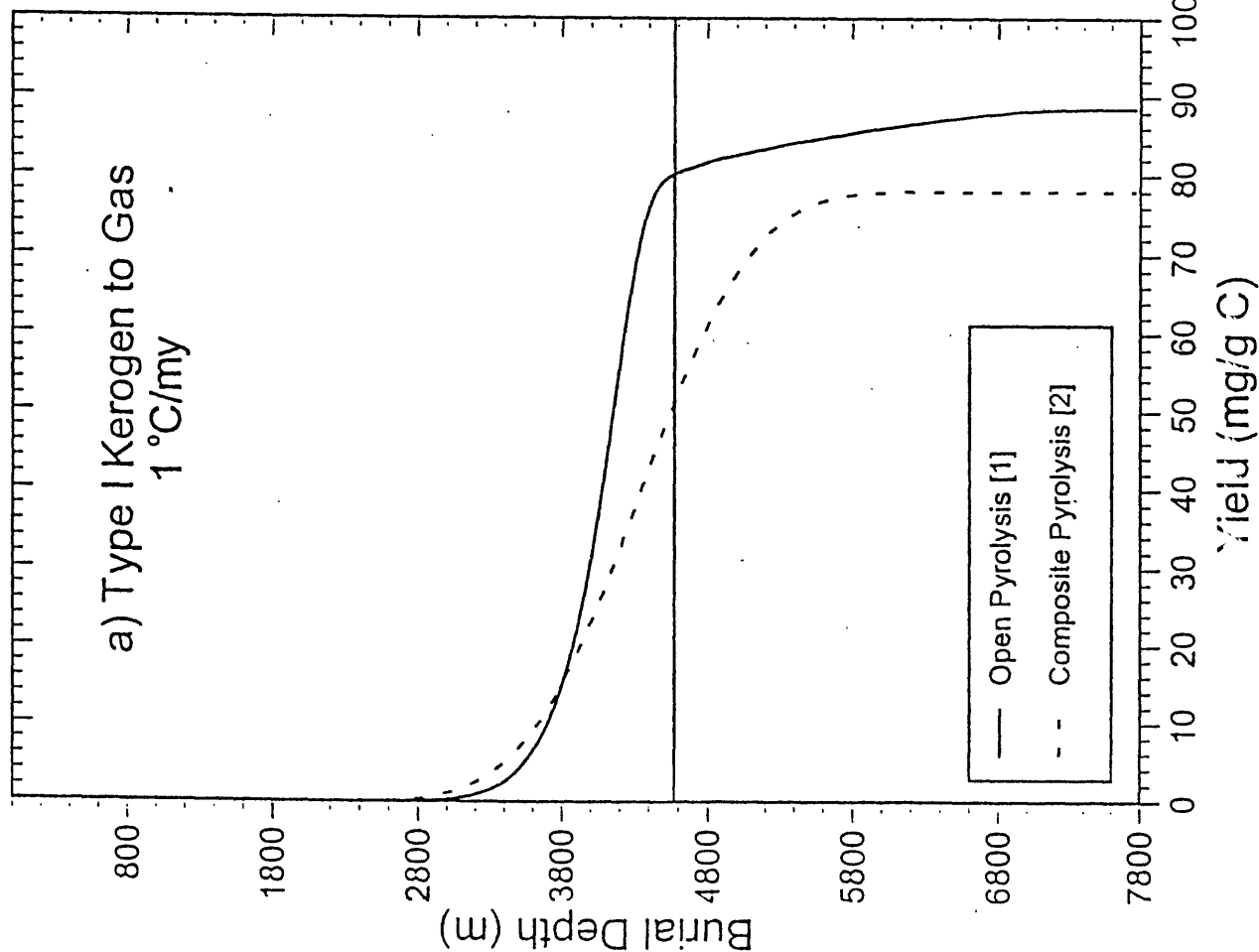
Figure 1: Amount of C_1-C_5 gas generated from Type-I kerogen with increasing burial depth according to the open-pyrolysis (solid line; [1]Behar and others, 1997) and composite-pyrolysis (dashed line; [2]Pepper and Corvi, 1995) models at geological heating rates of a) 1°C/m.y. and b)10°C/m.y. Deep-gas depths occur below the solid horizontal line drawn at 4,572 m.
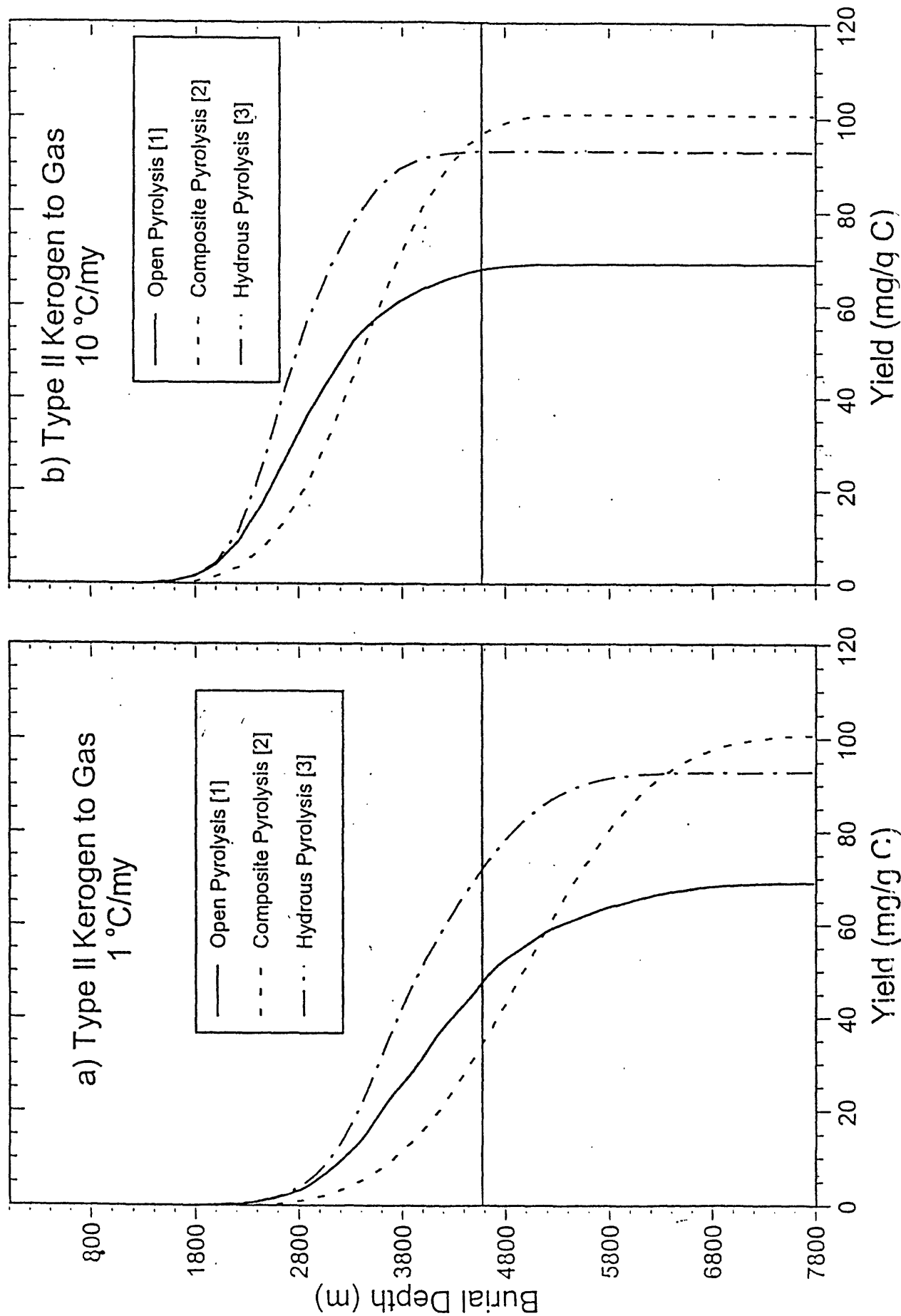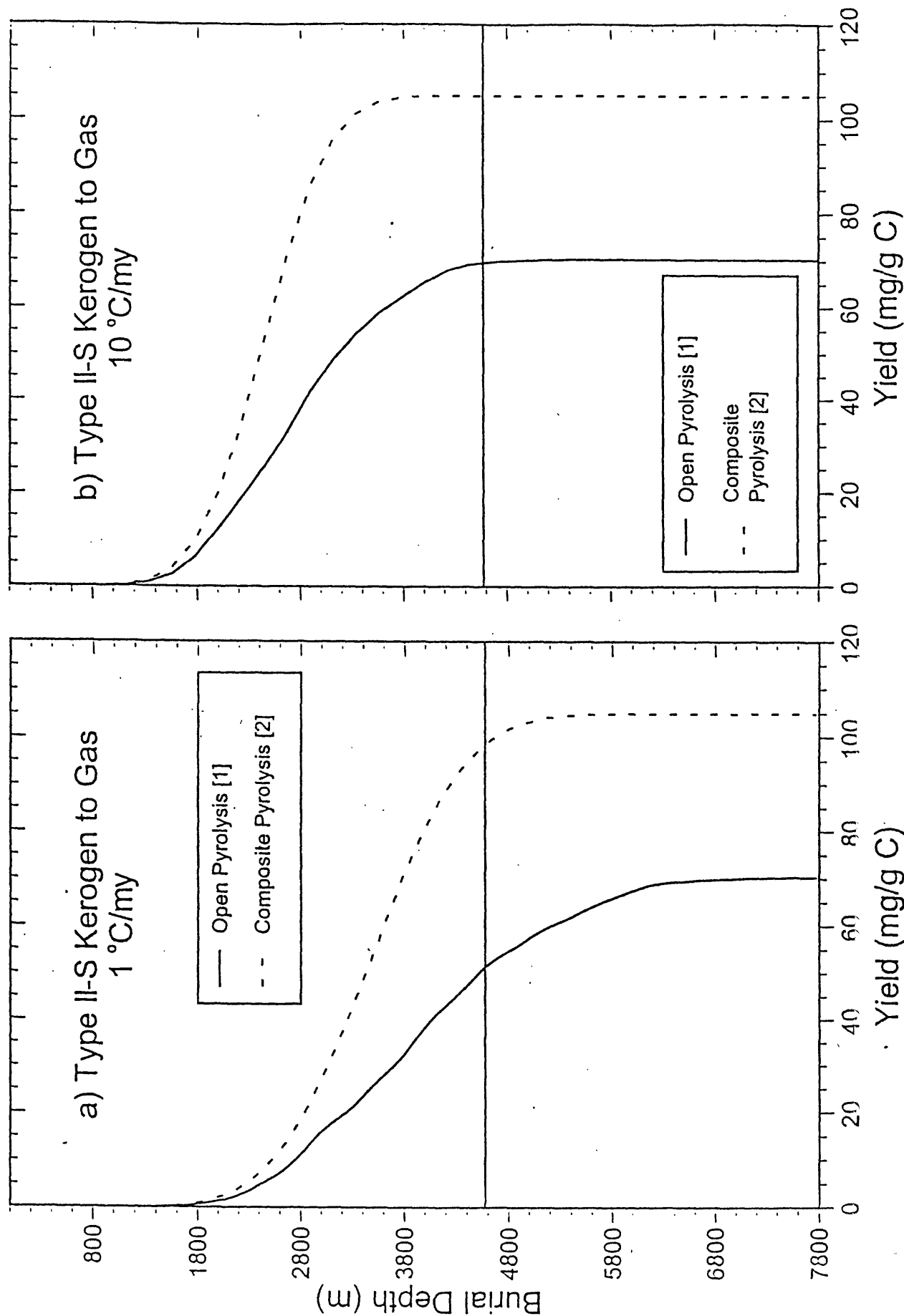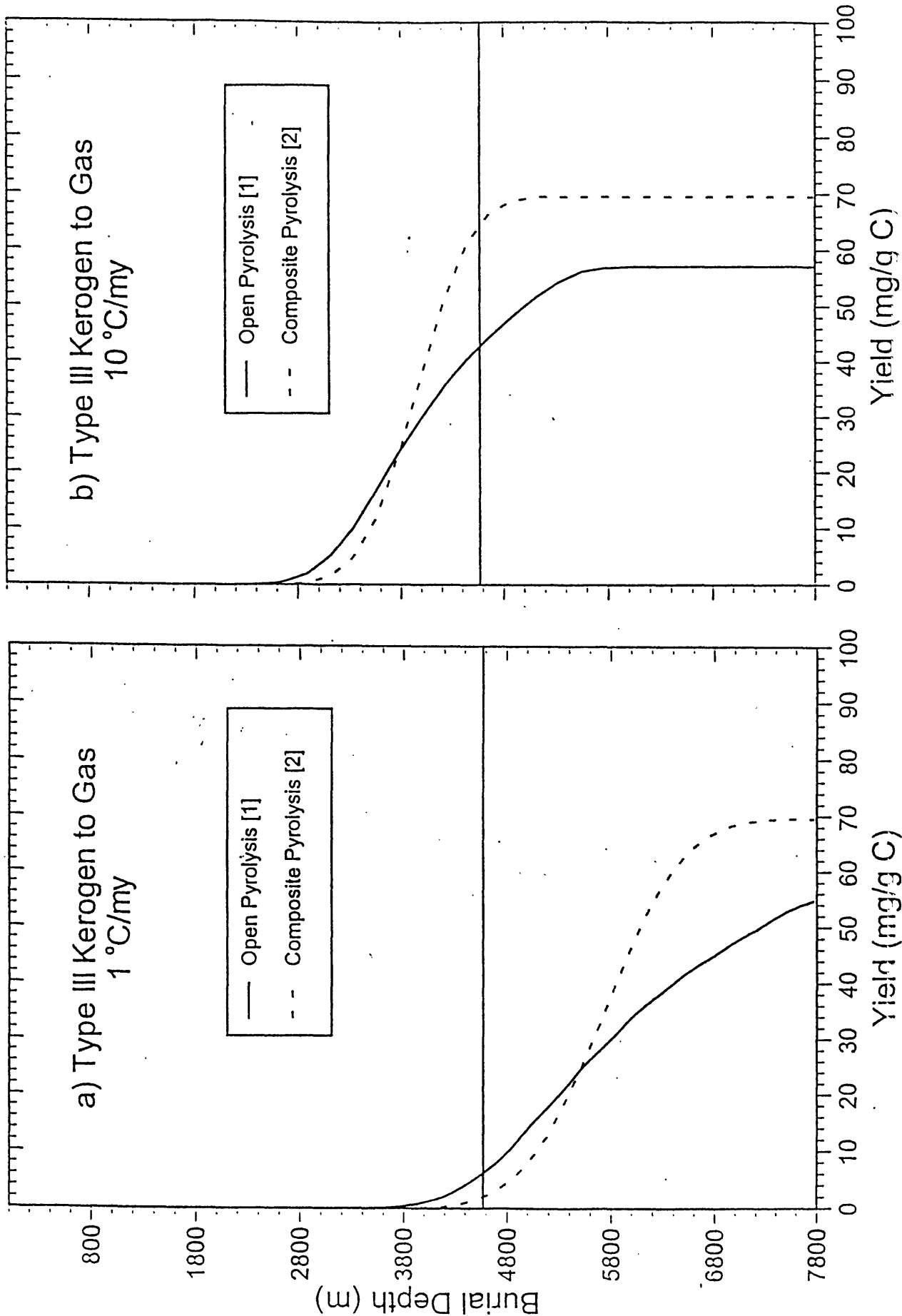
Figure 2: Amount of gas generated from Type-II kerogen with increasing burial depth according to the open-pyrolysis (solid line; C_1-C_5; [1]Behar and others, 1997), composite-pyrolysis (dashed line; C_1-C_5; [2]Pepper and Corvi, 1995), and hydrous-pyrolysis (dash-dot line; C_1-C_4; [3]Knauss and others, 1997) models at geological heating rates of **a)** 1°C/m.y. and **b)** 10°C/m.y. Deep-gas depths occur below the solid horizontal line drawn at 4,572 m.
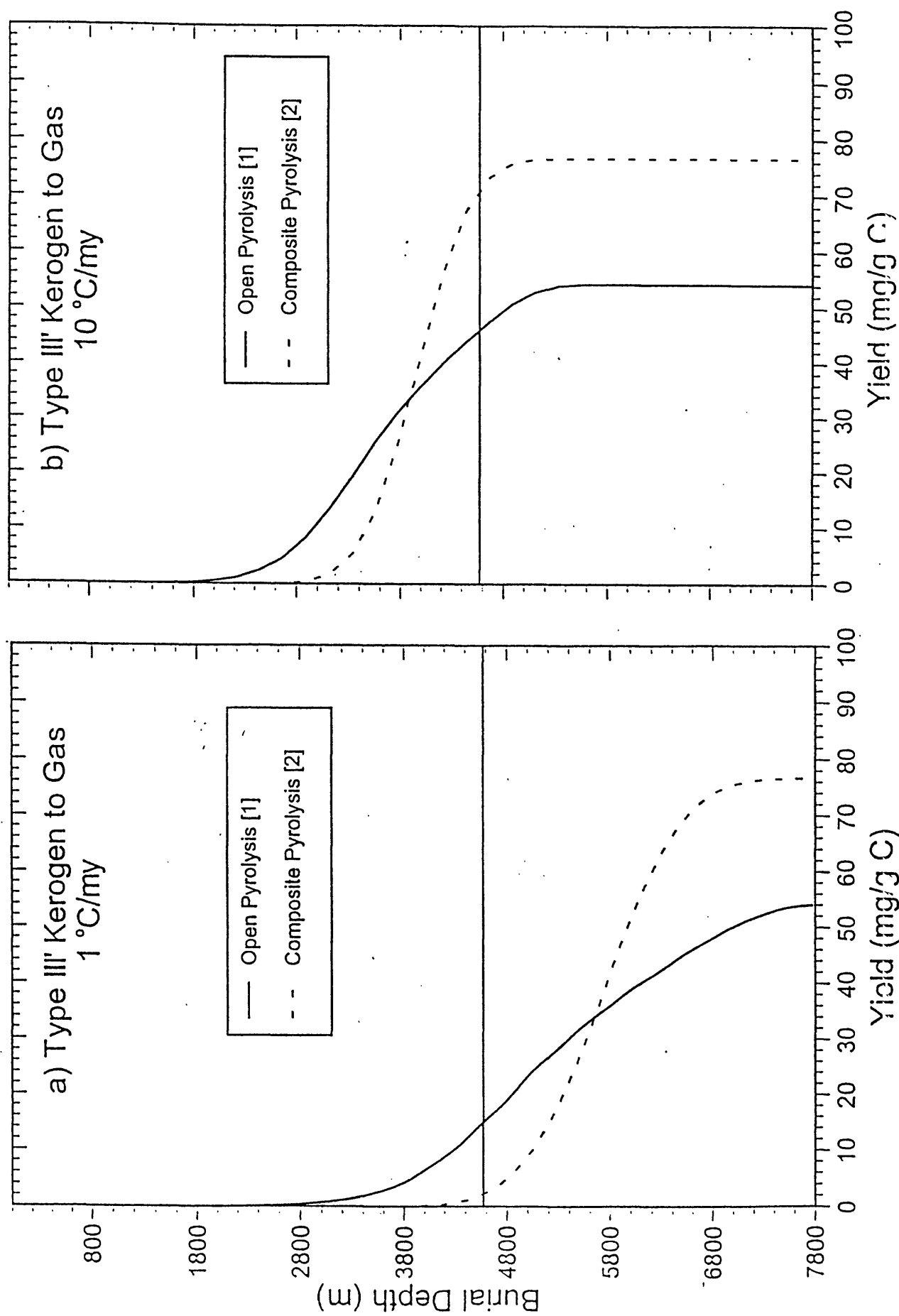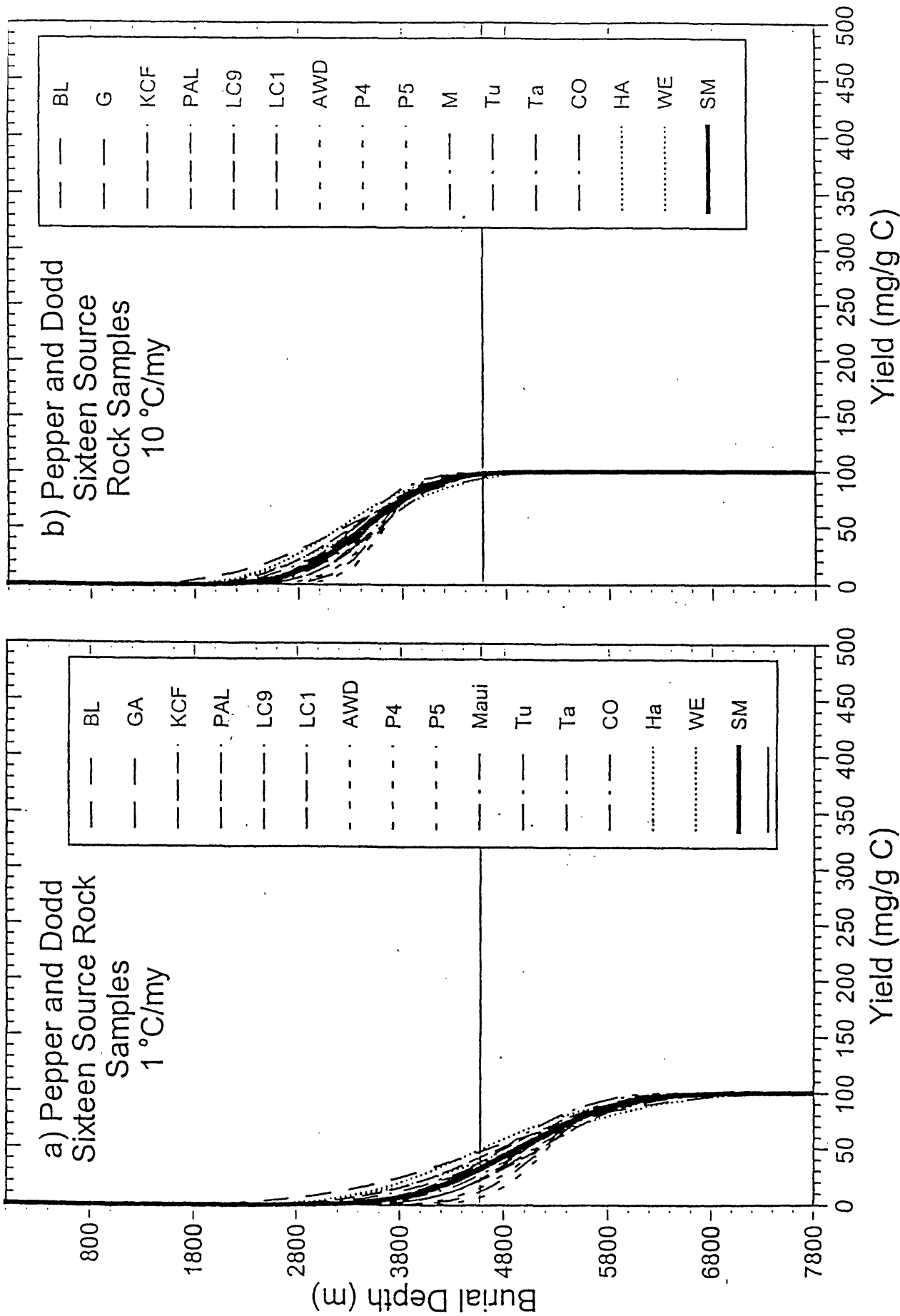
Figure 3: Amount of C_1-C_5 gas generated from Type-IIS kerogen with increasing burial depth according to the open-pyrolysis (solid line; [1]Behar and others, 1997) and composite-pyrolysis (dashed line; [2]Pepper and Corvi, 1995) models at geological heating rates of a) 1°C/m.y. and b)10°C/m.y. Deep-gas depths occur below the solid horizontal line drawn at 4,572 m.

Figure 4: Amount of C_1-C_5 gas generated from Type-III kerogen with increasing burial depth according to the open-pyrolysis (solid line; [1]Behar and others, 1997) and composite-pyrolysis (dashed line; [2]Pepper and Corvi, 1995) models at geological heating rates of a) 1°C/m.y. and b)10°C/m.y. Deep-gas depths occur below the solid horizontal line drawn at 4,572 m.

Figure 5: Amount of C_1-C_5 gas generated from Type-III' (paraffinic) kerogen with increasing burial depth according to the open-pyrolysis (solid line; [1]Behar and others, 1997) and composite-pyrolysis (dashed line; [2]Pepper and Corvi, 1995) models at geological heating rates of a) 1°C/m.y. and b)10°C/m.y. Deep-gas depths occur below the solid horizontal line drawn at 4,572 m.

Figure 6: Amount of C_1-C_5 gas generated from the cracking of oil in 16 different source rocks with increasing burial depth according to the anhydrous-pyrolysis model (solid lines; Pepper and Corvi, 1995) at geological heating rates of **a)** 1°C/m.y. and **b)** 10°C/m.y. Deep-gas depths occur below the solid horizontal line drawn at 4,572 m. Abbreviations for source rocks are **BL** = Brown Limestone, **SM** = St. Medard, **GA** = Garlin, **KCF** = not given, **PAL** = not given; **LC9** = LC995, **LC1** = LC1005, **AWD** = not given, **P4** = Pematang 45.2, **P5** = Pematang 52.7, **Maui** = Maui, **Tu** = Tuna, **Ta** = Tarakan, **CO** = COST, **Ha** = Haltenbanken, and **WE** = Westfield. The bold-solid St. Medard (SM) curve was selected to be the single representative gas-generation curve for all sixteen
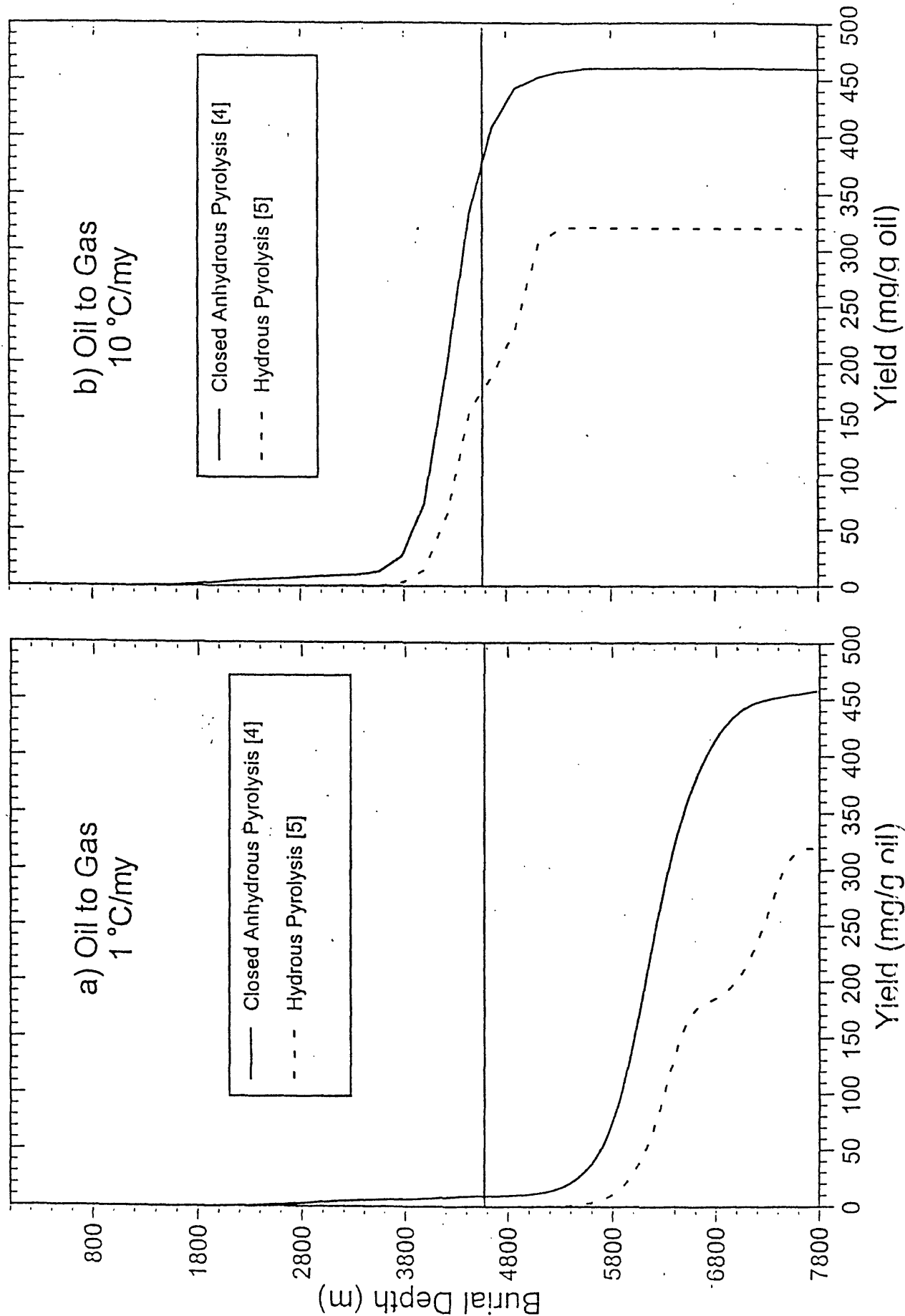
Figure 7: Amount of gas generated from the cracking of reservoir oil with increasing burial depth according to the anhydrous-pyrolysis (solid line; C$_1$-C$_4$; [4]Horsfield and others, 1992) and hydrous-pyrolysis (dash-dot line; C$_1$-C$_4$; [5]Tsuzuki and others, 1997) models at geological heating rates of a) 1°C/m.y. and b)10°C/m.y. Deep-gas depths occur below the solid horizontal line drawn at 4,572 m.